Noble-Gas-Induced Disproportionation Reactions: Facile Superoxo-to-Peroxo Conversion on Chromium Dioxide

Yanying Zhao,[†] Jing Su,[‡] Yu Gong,[†] Jun Li,*[,‡] and Mingfei Zhou*[,†]

Department of Chemistry, Shanghai Key Laboratory of Molecular Catalysts and Innovative Materials, Advanced Materials Laboratory, Fudan University, Shanghai 200433, P. R. China, and Department of Chemistry & Key Laboratory of Organic Optoelectronics and Molecular Engineering of Ministry of Education, Tsinghua University, Beijing 100084, P. R. China

Received: June 06, 2008; Revised Manuscript Received: July 17, 2008

Laser-evaporated chromium atoms are shown to insert into dioxygen to form CrO_2 in solid argon. Annealing allows diffusion and reactions to form $(\eta^2\text{-}O_2)_2CrO_2$, which is characterized as $[(O_2^-)_2(CrO_2)^{2+}]$, a side-on bonded disuperoxo−chromium dioxide complex. The $(\eta^2\text{-}O_2)_2CrO_2$ complex further reacts with xenon atom doped in solid argon to give $(\eta^1\text{-}OO)(\eta^2\text{-}O_2)CrO_2(Xe)$, which can be regarded as an O_2 molecule weakly interacting with $[(O_2)^{2-}(CrO_2)^{2+}Xe]$, a side-on bonded peroxo−chromium dioxide-xenon complex. The results indicate surprisingly that xenon atom induces a disproportionation reaction from superoxo to peroxo and dioxygen complex.

Introduction

Long after their discovery, noble gases were considered to be chemically inert due to the remarkable stability of the closed-shell electronic structure of the noble gas atoms in the ground state. As such, noble gases were applied to matrix isolation technique to trap and isolate free radicals and reactive intermediates for spectroscopic study.[1] It is generally assumed that the noble gas matrix that confines the free radicals and reactive intermediates is electronically innocent, such that the species trapped in the solid matrix were normally regarded as "isolated" molecules subject to weak polarizability-based "matrix effects".[2] However, noble gases are not completely chemically inert but exhibit a rich chemistry, particularly for the heavier elements, as first conjectured by Pauling.[3] A large number of chemically bound compounds containing noble gas atoms have been prepared since the report of $(Xe)PtF_6$.[3−9] Recent investigations indicate that some transition metal and actinide metal compounds were coordinated by one or multiple noble gas atoms in forming a variety of noble gas complexes in solid matrixes, which involves direct bonding interactions between metal and noble gas atoms.[10−13] The bindings of noble gas atoms to CUO and UO_2 cause an unusual *ground-state reversal* in the electronic state of the $CUO(Ng)_n$ and $UO_2(Ng)_n$ complexes.[10,12] While a large number of metal or nonmetal noble-gas compounds with direct chemical bonding have been reported,[3−13] there is no clear-cut evidence so far on the noble-gas-atom-mediated chemical reactions. Here we present a joint matrix isolation infrared spectroscopic and theoretical study to show that noble gas atoms can not only form direct chemical bonding with metals but also participate in the chemical process in noble gas matrix to induce a remarkable disproportionation reaction from a disuperoxo−chromium dioxide complex, $(\eta^2\text{-}O_2)_2CrO_2$ (**1**), to a rare noble-gas complex of peroxo−chromium dioxide, $(\eta^2\text{-}O_2)CrO_2(Xe)$, which exists in the frozen matrix as an O_2 weakly coordinated complex, $(\eta^1\text{-}OO)(\eta^2\text{-}O_2)CrO_2(Xe)$ (**2**). The formation of the xenon−chromium complexes via the noble-gas-induced disproportionation reactions provide an unprecedented example of the significant role played by noble-gas atoms in chemical reactions. These complexes may also serve as simple models for understanding the structure and bonding properties, and the reactivity of transition metal peroxo and superoxo complexes,[14] which are important reactive intermediates in numerous biological systems and catalytic oxidation reactions.[15,16]

Experimental and Computational Methods

The experimental setup for pulsed laser evaporation and matrix isolation infrared spectroscopic investigation has been described in detail previously.[17] Briefly, the 1064 nm fundamental of a Nd:YAG laser (Continuum, Minilite II, 10 Hz repetition rate and 6 ns pulse width) was focused onto a rotating chromium target through a hole in a CsI window cooled normally to 12 K by means of a closed-cycle helium refrigerator (ARS, 202N). The laser-evaporated chromium atoms were codeposited with oxygen/argon or oxygen/Xe/Ar mixtures onto the CsI window. In general, matrix samples were deposited for 1 h at a rate of approximately 4 mmol/h. The O_2/Ar and O_2/Xe/Ar mixtures were prepared in a stainless steel vacuum line using a standard manometric technique. Isotopic $^{18}O_2$ (ISOTEC, 99%) was used without further purification. The infrared absorption spectra of the resulting samples were recorded on a Bruker IFS 66V spectrometer at 0.5 cm^{-1} resolution between 4000 and 450 cm^{-1} using a liquid nitrogen cooled HgCdTe (MCT) detector. Samples were annealed at different temperatures and subjected to broad-band irradiation using a high-pressure mercury arc lamp with glass filters.

To validate the experimental assignment and to provide insights on the formation mechanism, structure, and bonding of the experimentally observed complexes, we performed density functional theory (DFT) and wave function theory (WFT) ab initio calculations. The DFT calculations were performed using the B3LYP functional and the 6-311+G(d) basis sets for oxygen and chromium atoms and the SDD pseudopotential and basis set for xenon atom.[18,19] The single point CCSD(T) energies of the structures optimized at the B3LYP level were calculated

* Corresponding authors. E-mail: junli@tsinghua.edu.cn (J.L.), mfzhou@fudan.edu.cn (M.Z.)
[†] Fudan University.
[‡] Tsinghua University.

10.1021/jp804995d CCC: $40.75
Published on Web 08/27/2008

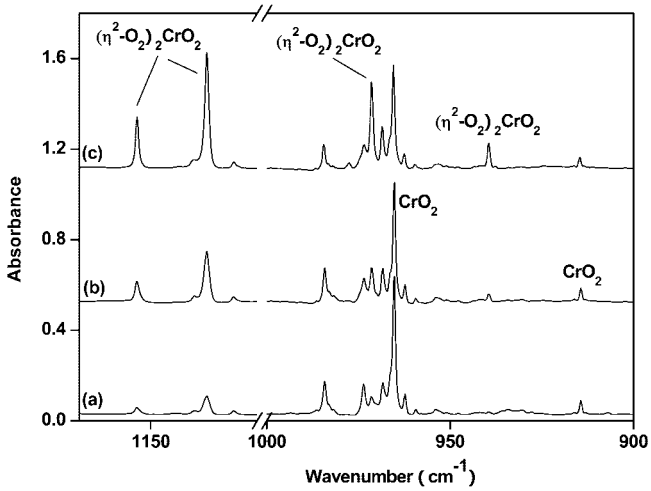

Figure 1. Infrared spectra in the 1170−1120 and 1000−900 cm^{-1} regions from codeposition of laser-evaporated chromium atoms with 2.0% O_2 in argon: (a) 1 h of sample deposition at 12 K, (b) after 25 K annealing, and (c) after 35 K annealing.

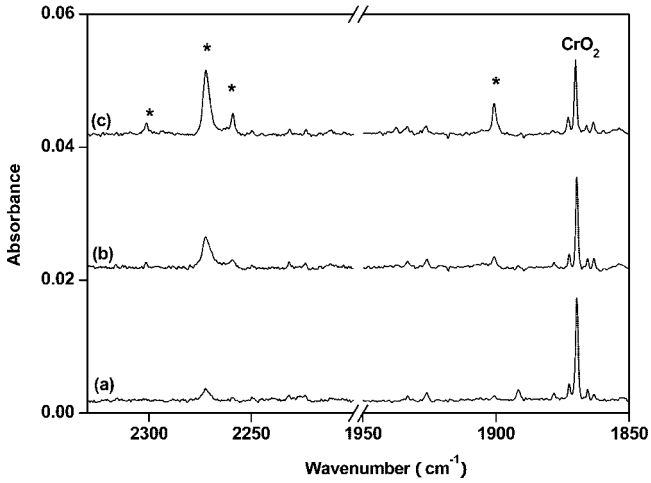

Figure 2. Infrared spectra in the 2330−2200 and 1950−1850 cm^{-1} regions from codeposition of laser-evaporated chromium atoms with 2.0% O_2 in argon: (a) 1 h of sample deposition at 12 K, (b) after 25 K annealing, and (c) after 35 K annealing. (The absorptions denoted with an asterisk are due to $(\eta^2\text{-}O_2)_2CrO_2$.)

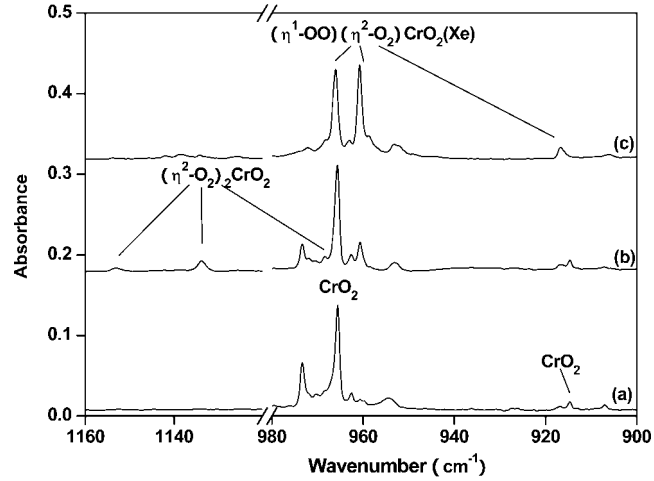

Figure 3. Infrared spectra in the 1160−1100 and 980−900 cm^{-1} regions from codeposition of laser-evaporated chromium atoms with 1% Xe + 2% O_2 in argon at 12 K: (a) 1 h of sample deposition at 12 K, (b) after annealing to 35 K, and (c) after annealing to 45 K.

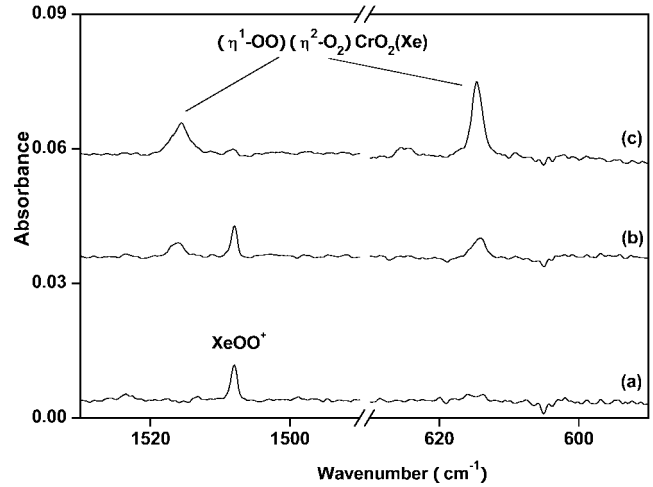

Figure 4. Infrared spectra in the 1530−1490 and 630−590 cm^{-1} regions from codeposition of laser-ablated chromium atoms with 1% Xe + 2% O_2 in argon at 12 K: (a) 1 h of sample deposition at 12 K, (b) after annealing to 35 K, (c) after annealing to 45 K, and (d) after annealing to 45 K.

using the same basis sets. All these calculations were performed by using the Gaussian 03 program.[20] The CASSCF and CASPT2 geometry optimizations were performed with SDD pseudopotentials and valence basis sets for Cr and Xe, with the 6-31+G* basis set for oxygen. These calculations were performed with MOLPRO 2006.1.[21]

Results and Discussion

The chromium oxide complexes were produced by codeposition of laser-evaporated chromium atoms with O_2/Ar and O_2/Xe/Ar mixtures. As shown in Figures 1 and 2, codeposition of laser-evaporated chromium atoms with 2.0% oxygen in argon at 12 K formed CrO_2 (ν_3, 965.4 cm^{-1}; ν_1, 914.4 cm^{-1}) as the major product, which has previously been identified from its infrared spectra and theoretical calculations.[22] Sample annealing decreased the CrO_2 absorptions and produced a new group of absorptions (group **A** hereafter) at 2301.2, 2272.1, 2259.1, 1900.7, 1153.9, 1134.2, 971.5, 939.6, and 532.0 cm^{-1}, which dominate the spectrum after high-temperature annealing. Similar experiments were performed with 1% Xe doped into the O_2/Ar mixture, and the spectra in selected regions are shown in Figures 3 and 4. Besides the aforementioned absorptions, the $XeOO^+$ absorption was observed after sample deposition,[23] and a new group of product absorptions at 1515.6, 966.3, 960.8, 916.6, and 614.6 cm^{-1} (group B) were produced on high-temperature annealing (35−45 K) at the expense of the group A absorptions. Isotopic substitutions ($^{18}O_2$, and $^{16}O_2$ + $^{18}O_2$ mixture) were employed for product identification, and the new product absorptions are listed in Table 1 with the isotopic spectra in selected regions shown in Figures 5,6, and 7, respectively.

The group A absorptions maintain the same relative intensities throughout all the experiments and are assigned to different vibrational modes of the $(\eta^2\text{-}O_2)_2CrO_2$ complex (Table 1). The 971.5, 1134.2, and 1153.9 cm^{-1} absorptions were initially assigned to $OOCrO_2$, OOCrOO, and CrOO, respectively,[22] but were reassigned to the $(O_2)_2CrO_2$ molecule based on further experiments.[24] The 971.5 and 939.6 cm^{-1} absorptions shift to 934.7 and 898.3 cm^{-1} with $^{18}O_2$, which yield $^{16}O/^{18}O$ isotopic frequency ratios of 1.0394 and 1.0460, respectively. The band positions and isotopic frequency ratios imply that these two absorptions are due to the antisymmetric and symmetric OCrO

TABLE 1: Infrared Absorptions (cm^{-1}) of the $(\eta^2\text{-}O_2)_2CrO_2$ and $(\eta^1\text{-}OO)(\eta^2\text{-}O_2)CrO_2(Xe)$ Complexes in Solid Argon

$^{16}O_2$	$^{18}O_2$	$^{16}O_2 + {}^{18}O_2$	assignment
2301.2			$(\eta^2\text{-}O_2)_2CrO_2$ $2\nu_1$
2272.1	2142.6		$(\eta^2\text{-}O_2)_2CrO_2$ $\nu_1 + \nu_{12}$
2259.1	2133.2		$(\eta^2\text{-}O_2)_2CrO_2$ $2\nu_{12}$
1900.7	1823.3		$(\eta^2\text{-}O_2)_2CrO_2$ $\nu_2 + \nu_9$
1153.9	1090.8	1153.9, 1145.4, 1090.8	$(\eta^2\text{-}O_2)_2CrO_2$ ν_1 (sym O−O str)
1134.2	1070.8	1134.2, 1078.3, 1070.8	$(\eta^2\text{-}O_2)_2CrO_2$ ν_{12} (asym O−O str)
977.5	940.8		$(\eta^2\text{-}O_2)_2{}^{50}CrO_2$ ν_9
971.5	934.7	971.5, 934.7	$(\eta^2\text{-}O_2)_2{}^{52}CrO_2$ ν_9 (asym CrO_2 str)
968.7	931.3		$(\eta^2\text{-}O_2)_2{}^{53}CrO_2$ ν_9
965.8			$(\eta^2\text{-}O_2)_2{}^{54}CrO_2$ ν_9
943.4	902.4		$(\eta^2\text{-}O_2)_2{}^{50}CrO_2$ ν_2
939.6	898.3	939.6, 898.3	$(\eta^2\text{-}O_2)_2{}^{52}CrO_2$ ν_2 (sym CrO_2 str)
937.6	896.1		$(\eta^2\text{-}O_2)_2{}^{53}CrO_2$ ν_2
935.8	894.1		$(\eta^2\text{-}O_2)_2{}^{54}CrO_2$ ν_2
532.0	511.7		$(\eta^2\text{-}O_2)_2CrO_2$ ν_{13} (asym Cr−O_2 str)
1515.6	1430.6	1519.8, 1515.5, 1434.1, 1430.6	$(\eta^1\text{-}OO)(\eta^2\text{-}O_2)CrO_2(Xe)$ O−O str
966.3	929.7	966.3, 954.1, 929.7	$(\eta^1\text{-}OO)(\eta^2\text{-}O_2)CrO_2(Xe)$ asym CrO_2 str
960.8	920.0	960.8. 941.0, 920.0	$(\eta^1\text{-}OO)(\eta^2\text{-}O_2)CrO_2(Xe)$ (sym CrO_2 str)
916.6	860.7	916.6, 869.6, 860.7	$(\eta^1\text{-}OO)(\eta^2\text{-}O_2)CrO_2(Xe)$ O−O str
614.6	586.1	617.0, 614.6, 586.5, 586.1	$(\eta^1\text{-}OO)(\eta^2\text{-}O_2)CrO_2(Xe)$ Cr−O_2 str

stretching vibrations. These absorptions and additional weak satellite features at 977.5/968.7/965.8 and 943.4/937.6/935.8 cm^{-1} (Table 1) show natural abundance chromium isotopic intensity distributions and clearly indicate the involvement of one chromium atom. The 1153.9 and 1134.2 cm^{-1} absorptions shift to 1090.8 and 1070.8 cm^{-1} upon ^{18}O substitution. The band positions and $^{16}O/^{18}O$ isotopic frequency ratios of 1.0578 and 1.0592 are characteristic of the O−O stretching vibrations of superoxo ligands.[25,26] The spectra with a $^{16}O_2 + {}^{18}O_2$ mixture (Figure 5) clearly indicate that two equivalent O_2 subunits are involved in these modes. The much weaker 532.0 cm^{-1} absorption is due to the Cr−O_2 stretching mode. The observation of overtone and combination modes above 1900 cm^{-1} (Table 1) lends additional credence on the assignment.

The group B absorptions appear only in the xenon-doped experiments at the expense of the $(\eta^2\text{-}O_2)_2CrO_2$ absorptions and are assigned to the $(\eta^1\text{-}OO)(\eta^2\text{-}O_2)CrO_2(Xe)$ complex. The 1515.6 cm^{-1} absorption exhibits a $^{16}O/^{18}O$ isotopic frequency ratio of 1.0594 and is due to the O−O stretching vibration of a very weakly bound dixoygen complex based on the band position and isotopic frequency ratio. In contrast, free O_2 adsorbs at 1580.2 cm^{-1} in the gas phase and at 1553 cm^{-1} in solid argon.[27] The 916.6 cm^{-1} absorption exhibits the $^{18}O_2$ counterpart at 860.7 cm^{-1}. The band position and $^{16}O/^{18}O$ frequency ratio (1.0649) indicate that this band is due to the O−O stretching vibration of a peroxide ligand.[25,26] The 966.3 and 960.8 cm^{-1} absorptions shift to 929.7 and 920.0 cm^{-1} with $^{18}O_2$. The $^{16}O/^{18}O$ frequency ratios of 1.0394 and 1.0443 are appropriate for the antisymmetric and symmetric OCrO stretching vibrations. The 614.6 cm^{-1} absorption is due to the Cr−O_2 stretching vibration of the complex.

The optimized DFT geometries of $(\eta^2\text{-}O_2)_2CrO_2$ and $(\eta^1\text{-}OO)(\eta^2\text{-}O_2)CrO_2(Xe)$ are shown in Figure 8, and the calculated harmonic vibrational frequencies and $^{16}O/^{18}O$ isotopic frequency ratios are listed in Tables 2 and 3. As vibrational frequencies tend to be reduced (i.e., red-shifted) by the argon matrix relative to those in gas phase, the calculated vibrational frequencies and isotopic frequency ratios are in reasonable agreement with the experimental values, which provide strong support to the experimental assignment.

The $(\eta^2\text{-}O_2)_2CrO_2$ complex is predicted to have a $^3B_2$ ground-state with a tetrahedral skeleton of C_{2v} symmetry, in which the

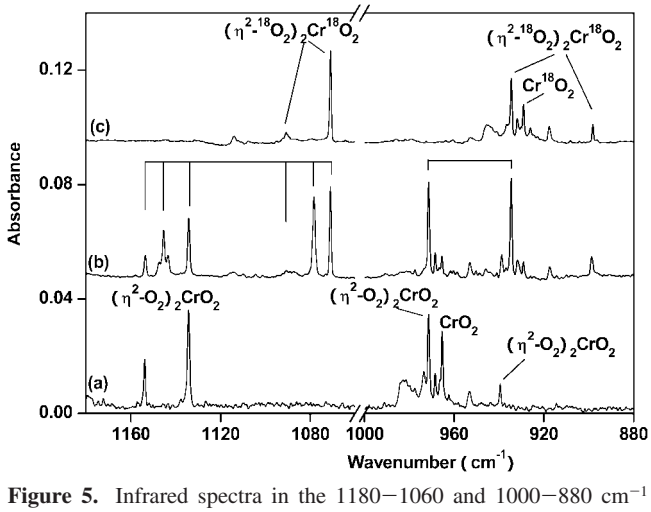

Figure 5. Infrared spectra in the 1180−1060 and 1000−880 cm^{-1} regions from codeposition of laser-ablated chromium atoms with isotopically substituted O_2 in excess argon at 12 K; spectra were taken after 1 h of sample deposition followed by 45 K annealing: (a) 2.0% $^{16}O_2$, (b) 1.5% $^{16}O_2$ + 1.5% $^{18}O_2$, and (c) 2.0% $^{18}O_2$.

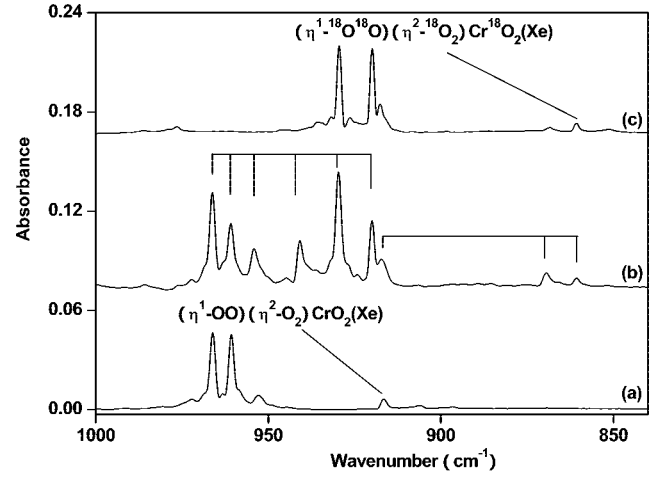

Figure 6. Infrared spectra in the 1000−840 cm^{-1} region from codeposition of laser-ablated chromium atoms with isotopically substituted O_2 in a xenon-doped argon matrix; spectra were taken after 1 h of sample deposition followed by 45 K annealing: (a) 1% Xe + 2.0% $^{16}O_2$, (b) 1% Xe+ 1.5% $^{16}O_2$ + 1.5% $^{18}O_2$, and (c) 1% Xe + 2.0% $^{18}O_2$.

TABLE 2: Vibrational Frequencies (cm^{-1}) and Intensities (km/mol) of the Complexes Calculated at the B3LYP/6-311+G* Level

complex	frequency (mode, intensity)
(η^2-O_2)$_2$$CrO_2$ (C_{2v}, $^3B_2$)	1249.2 (a_1, 57), 1230.0 (b_2, 158), 1070.8 (b_1, 256), 1049.4 (a_1, 70), 583.0 (a_1, 1), 547.5 (b_2, 36), 374.7 (a_1, 1), 337.2 (a_1, 0), 324.5 (b_2, 1), 294.5 (a_2, 0), 252.8 (b_1, 0), 218.3 (b_1, 3), 192.5 (b_2, 31), 176.2 (a_1,0), 167.8 (a_2, 0)
(η^1-OO) (η^2-O_2)CrO_2(Xe) (C_s, $^3A''$)	1633.8 (0.1, a′), 1074.8 (192, a″), 1061.5 (143, a′), 986.7 (63, a′), 642.1 (40, a′), 600.2 (4, a′), 370.6 (0, a′), 277.5 (1, a″), 271.6 (64, a′), 194.9 (0, a″), 115.1 (0, a′), 113.9 (0, a″), 92.4 (3, a′), 41.5 (0, a′), 29.5 (0, a″), 18.9 (0, a′), 8.2 (1, a′), 8.0 (0, a″)
(η^2-O_2)CrO_2(Xe) (C_s, $^1A'$)	1074.8 (196, a″), 1061.5 (144, a′), 986.2 (64, a′), 642.6 (37, a′), 600.1 (4, a′), 370.4 (0, a′), 277.6 (1, a″), 272.4 (60, a′), 194.1 (0, a″), 114.2 (0, a′), 112.1 (0, a″), 93.1 (2, a′)

two O_2 fragments lie in the same plane that is perpendicular to the OCrO plane. The two η^2-O_2 fragments are equivalent and bound in an asymmetric, side-on fashion, with two inequivalent Cr−O bond lengths of 2.038 and 1.918 Å, respectively. The predicted O−O bond lengths of the two O_2 subunits (1.292 Å) fall into the superoxide category.[25,26] Therefore, the (η^2-O_2)$_2$$CrO_2$ complex can be regarded as a side-on bonded disuperoxo−chromium dioxide complex, [$(O_2^-)_2(CrO_2)^{2+}$], where two O_2^- anions bound to a CrO_2^{2+} dication. Consistent with the above notion, the two unpaired electrons in the $^3B_2$ ground state of the (η^2-O_2)$_2$$CrO_2$ complex occupy the $7b_1$ and $3a_2$ molecular orbitals, which are primarily antibonding π^* orbitals of the two O_2^- subunits in character (Figure 9). The calculated spin densities are localized on the two O_2^- subunits, with $0.45e^-$ and $0.59e^-$ for the two O atoms in each O_2^-.

The (η^1-OO)(η^2-O_2)CrO_2(Xe) complex was predicted to have C_s symmetry and $^3A''$ ground-state with the two O_2 fragments and xenon atom in the same plane that is perpendicular to the OCrO plane (Figure 8). The end-on bonded η^1-OO fragment

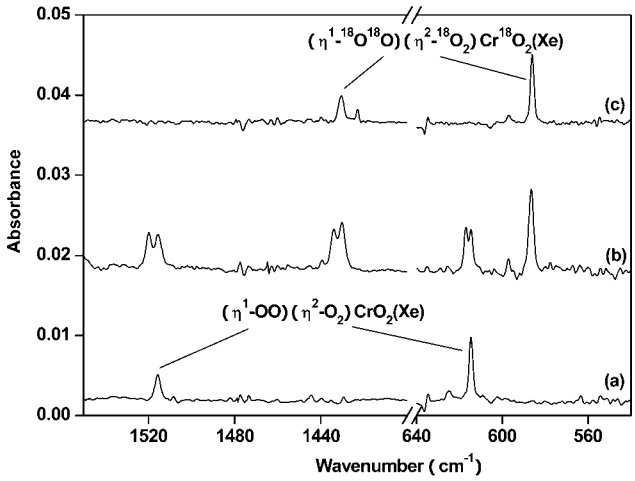

Figure 7. Infrared spectra in the 1550−1400 and 640−540 cm^{-1} regions from codeposition of laser-ablated chromium atoms with isotopically substituted O_2 in xenon-doped argon matrix; spectra were taken after 1 h of sample deposition followed by 45 K annealing: (a) 1% Xe + 2.0% $^{16}O_2$, (b) 1% Xe+ 1.5% $^{16}O_2$ + 1.5% $^{18}O_2$, and (c) 1% Xe + 2.0% $^{18}O_2$.

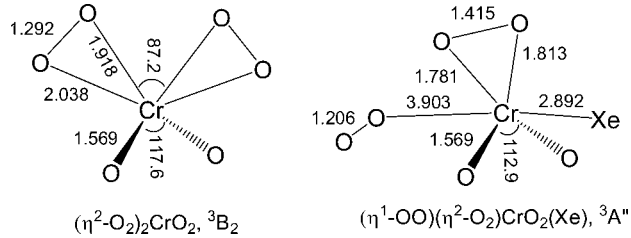

Figure 8. Calculated structures of the (η^2-O_2)$_2$$CrO_2$ (**1**) and (η^1-OO)(η^2-O_2)CrO_2(Xe) (**2**) complexes. Listed are the bond lengths (Å) and bond angles (deg) from B3LYP geometry optimizations.

TABLE 3: Comparison between the Observed and Calculated Vibrational Frequencies (cm^{-1}) and Isotopic Frequency Ratios for the (η^2-O_2)$_2$$CrO_2$ (1) and (η^1-OO)(η^2-O_2)CrO_2(Xe) (2) Complexes

exptl		calcd[a]		
ν	$^{16}O/^{18}O$	ν	$^{16}O/^{18}O$	mode
2301.2		2418.2		**1** $2\nu_1$
2272.1	1.0604	2401.6		**1** $\nu_1 + \nu_{12}$
2259.1	1.0590	2385.0		**1** $2\nu_{12}$
1900.7	1.0425	2052.1		**1** $\nu_2 + \nu_9$
1153.9	1.0578	1209.1	1.0608	**1** ν_1 (sym O−O str)
1134.2	1.0592	1192.5	1.0606	**1** ν_{12} (asym O−O str)
971.5	1.0394	1036.4	1.0395	**1** ν_9 (asym $^{52}CrO_2$ str)
939.6	1.0460	1015.7	1.0478	**1** ν_2 (sym $^{52}CrO_2$ str)
532.0	1.0397	529.9	1.0360	**1** ν_{13} (asym Cr−O_2 str)
1515.6	1.0594	1581.4	1.0608	**2** O−O str
966.3	1.0394	1040.3	1.0398	**2** asym CrO_2 str
960.8	1.0443	1027.4	1.0456	**2** sym CrO_2 str
916.6	1.0649	955.0	1.0599	**2** O−O str
614.6	1.0486	621.5	1.0497	**2** Cr−O_2 str

[a] The calculated B3LYP/6−311+G(d) frequencies are scaled by 0.9679; see ref 31.

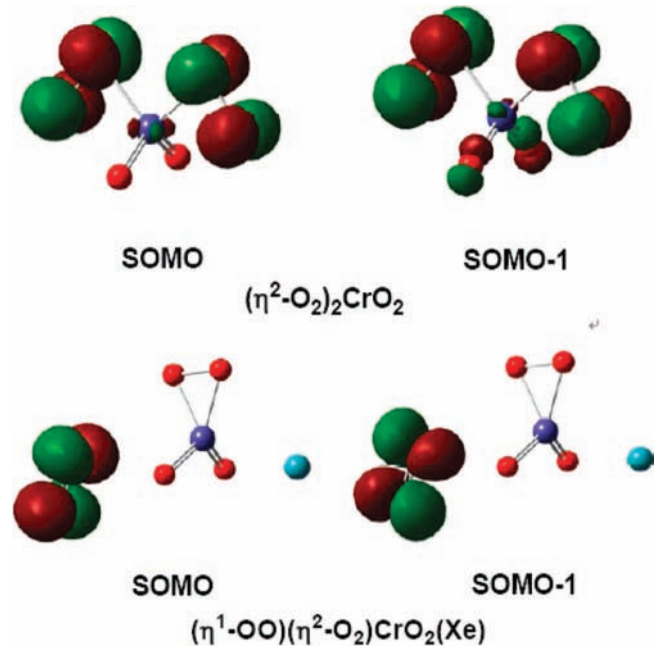

Figure 9. The 3D contours of the singly occupied molecular orbitals of the observed complexes.

was predicted to have an O−O bond length of 1.206 Å, which is about the same as that of free O_2, while the Cr−OO distance was calculated to be rather long (3.903 Å) at the B3LYP level. Therefore, the complex can be regarded as a triplet O_2 molecule adsorbed on a closed-shell (η^2-O_2)CrO_2(Xe) complex. As can be seen in Table 2, the calculated vibrational frequency differences between (η^2-O_2)CrO_2(Xe) and (η^1-OO)(η^2-O_2)-

$CrO_2(Xe)$ are less than one wavenumber. The O−O distance in the $(\eta^2\text{-}O_2)CrO_2(Xe)$ fragment was calculated to be 1.415 Å, which is typical of peroxide complexes.[25,26] The $(\eta^2\text{-}O_2)CrO_2(Xe)$ fragment can be characterized as $[(O_2)^{2-}(CrO_2)^{2+}\text{-}Xe]$, a side-on bonded peroxo−chromium dioxide−xenon complex. Indeed, the calculated unpaired spin resides on the adsorbed dioxygen molecule with $0.98e^-$ and $1.01e^-$ for the two O atoms. The Cr−Xe bond has a theoretically optimized bond distance of 2.892 Å and a binding energy of 14.0 kcal/mol with respect to the $(O_2)CrO_2$ ($^1A_1$) + Xe asymptotes at the CCSD(T)//B3LYP level after zero point energy correction, which are comparable with those previously reported transition-metal−Xe complexes.[28−30] As weak interactions between O_2 or Xe and $(\eta^2\text{-}O_2)CrO_2$ are expected to be poorly described by DFT methods, the calculated OO−Cr and Cr−Xe bond distances are only qualitative. Further geometry optimizations were performed using ab initio CASSCF (complete-active-space self-consistent-field) and CASPT2 (complete-active-space second-order perturbation theory) methods. The OO−Cr and Cr−Xe distances are 3.849 and 3.176 Å at the level of CASSCF calculations and 3.238 and 2.708 Å at the level of CASPT2 calculations. The OO−Cr and Cr−Xe bond distances calculated at the CASPT2 level are indeed significantly shorter than those predicted by the DFT methods, indicating that dynamic electron correlations have contributed significantly to the weak interaction between OO or Xe and the $(\eta^2\text{-}O_2)CrO_2$ unit.

The spectra in Figure 1 clearly demonstrate that chromium dioxide reacts with molecular oxygen in solid argon to form the side-on bonded disuperoxo−chromium dioxide complex **1**. One of the superoxo ligands of the complex can be replaced by a xenon atom doped in solid argon via an S_N2-type substitution reaction to form the side-on bonded peroxo−chromium dioxide−xenon complex and releases one molecular dioxygen, which cannot escape the matrix "cage" and survived as the weakly bound complex **2**. In this process, one of the superoxo anion radicals in $(\eta^2\text{-}O_2)_2CrO_2$ (with two O−O stretch frequencies at 1153.9 and 1134.2 cm^{-1}) was reduced to a peroxo ion (with the O−O stretch frequency at 916.6 cm^{-1}), whereas another superoxo anion radical is oxidized to a molecular dioxygen. Therefore, this process represents a remarkable example of xenon-atom-induced disproportionation reactions, which is predicted to be exothermic by 7.4 kcal/mol at the CCSD(T)//B3LYP level of theory after zero point energy correction. The chemical transformation of superoxide ions to dioxygen and peroxo complexes bears resemblance to the dismutation of superoxide ion via catalytic superoxide dismutatase protein. The above-characterized $(\eta^2\text{-}O_2)_2CrO_2$ (**1**) and $(\eta^1\text{-}OO)(\eta^2\text{-}O_2)CrO_2(Xe)$ (**2**) molecules can therefore be regarded as model complexes demonstrating the O_2 activation through electron transfer from metal oxides to form the superoxo complexes and further convert to dioxygen and peroxo complexes.

Conclusions

A joint matrix isolation infrared spectroscopic and theoretical study was performed to show that noble-gas atoms are able to participate in the chemical process in noble-gas matrix to induce a remarkable disproportionation reaction from disuperoxo to peroxo and dioxygen complexes. These complexes were produced by codeposition of laser-evaporated chromium atoms with O_2/Ar and O_2/Xe/Ar mixtures. The chromium atoms insert into dioxygen to form the previously characterized CrO_2 molecules in solid argon, which further react with dioxygen to give the $(\eta^2\text{-}O_2)_2CrO_2$ complex, a side-on bonded disuperoxo−chromium dioxide complex. The $(\eta^2\text{-}O_2)_2CrO_2$ complex further reacts with xenon atom doped in solid argon to give the noble-gas complex of peroxo−chromium dioxide, $(\eta^2\text{-}O_2)CrO_2(Xe)$, which exists in the frozen matrix as an O_2 weakly coordinated complex, $(\eta^1\text{-}OO)(\eta^2\text{-}O_2)CrO_2(Xe)$.

Acknowledgment. This work was supported by NKBRSF (2007CB815203, 2006CB932300) and NNSFC (20773030, 20525104, and 20433080) of China, and the calculations were performed by using a HP Itanium2 cluster at Tsinghua National Laboratory for Information Science and Technology.

References and Notes

(1) Whittle, E.; Dows, D. A.; Pimentel, G. C. *J. Chem. Phys.* **1954**, *22*, 1943.

(2) (a) Jacox, M. E. *Chem. Phys.* **1994**, *189*, 149. (b) Jacox, M. E. *Chem. Soc. Rev.* **2002**, *31*, 108. (c) Jacox, M. E. *J. Phys. Chem. Ref. Data* **2003**, *32*, 1.

(3) (a) Pauling, L. *J. Am. Chem. Soc.* **1933**, *55*, 1895. (b) Gerber, R. B. *Annu. Rev. Phys. Chem.* **2004**, *55*, 57. (c) Christe, K. O. *Angew. Chem., Int. Ed.* **2001**, *40*, 1419. (d) Pyykkö, P. *Science* **2000**, *290*, 64. (e) Lehmann, J. F.; Mercier, H. P. A.; Schrobilgen, G. J. *Coord. Chem. Rev.* **2002**, *233*, 1. (f) Petterson, M.; Lundell, J.; Räsänen, M *Eur. J. Inorg. Chem.* **1999**, 729. (g) Holloway, J. H.; Hope, E. G. *Adv. Inorg. Chem.* **1999**, *46*, 51.

(4) Bartlett, N. *Proc. Chem. Soc.* **1962**, 218.

(5) Turner, J. J.; Pimentel, G. C. *Science* **1963**, *140*, 974.

(6) Khriachtchev, L.; Pettersson, M.; Runeberg, N.; Lundell, J.; Räsänen, M. *Nature* **2000**, *406*, 874.

(7) Seidel, S.; Seppelt, K. *Science* **2000**, *290*, 117.

(8) (a) Khriachtchev, L.; Tanskanen, H.; Cohen, A.; Gerber, R. B.; Lundell, J.; Pettersson, M.; Kiljunen, H.; Räsänen, M. *J. Am. Chem. Soc.* **2003**, *125*, 6876. (b) Khriachtchev, L.; Tanskanen, H.; Lundell, J.; Pettersson, M.; Kiljunen, H.; Räsänen, M. *J. Am. Chem. Soc.* **2003**, *125*, 4696.

(9) (a) Evans, C. J.; Lesarri, A.; Gerry, M. C. L. *J. Am. Chem. Soc.* **2000**, *122*, 6100. (b) Cooke, S. A.; Gerry, M. C. L. *J. Am. Chem. Soc.* **2004**, *126*, 17000.

(10) Li, J.; Bursten, B. E.; Liang, B. Y.; Andrews, L. L. *Science* **2002**, *295*, 2242.

(11) (a) Andrews, L.; Liang, B. Y.; Li, J.; Bursten, B. E. *J. Am. Chem. Soc.* **2003**, *125*, 3126. (b) Andrews, L.; Liang, B. Y.; Li, J.; Bursten, B. E. *Angew. Chem., Int. Ed.* **2000**, *39*, 4565.

(12) (a) Li, J.; Bursten, B. E.; Andrews, L.; Marsden, C. J. *J. Am. Chem. Soc.* **2004**, *126*, 3424. (b) Wang, X. F.; Andrews, L.; Li, J.; Bursten, B. E. *Angew. Chem., Int. Ed.* **2004**, *43*, 2554.

(13) (a) Zhao, Y. Y.; Wang, G. J.; Chen, M. H.; Zhou, M. F. *J. Phys. Chem. A* **2005**, *109*, 6621. (b) Zhao, Y. Y.; Gong, Y.; Chen, M. H.; Ding, C. F.; Zhou, M. F. *J. Phys. Chem. A* **2005**, *109*, 11765. (c) Zhao, Y. Y.; Gong, Y.; Chen, M. H.; Zhou, M. F. *J. Phys. Chem. A* **2006**, *110*, 1845. (d) Zhao, Y. Y.; Gong, Y.; Zhou, M. F. *J. Phys. Chem. A* **2006**, *110*, 10777. (e) Yang, R.; Gong, Y.; Zhou, H.; Zhou, M. F *J. Phys. Chem. A* **2007**, *111*, 64. (f) Yang, R.; Gong, Y.; Zhou, M. F. *Chem. Phys.* **2007**, *240*, 134.

(14) See for example:(a) Qin, K.; Incarvito, C. D.; Rheingold, A. L.; Theopold, K. H. *Angew. Chem., Int. Ed.* **2002**, *41*, 2333. (b) Huang, X.; Zhai, H. J.; Waters, T.; Li, J.; Wang, L. S. *Angew. Chem., Int. Ed.* **2006**, *45*, 657. (c) Zhai, H. J.; Kiran, B.; Cui, L. F.; Li, X.; Dixon, D. A.; L. S; Wang, J. *Am. Chem. Soc* **2004**, *126*, 16134.

(15) (a) Levina, A.; Lay, P. A. *Coord. Chem. Rev.* **2005**, *249*, 281. (b) Bakac, A.; Wang, W. D. *J. Am. Chem. Soc.* **1996**, *118*, 10325.

(16) (a) Dyrek, K.; Che, M. *Chem. Rev.* **1997**, *97*, 305. (b) Giamello, E. *Catal. Today* **1998**, *41*, 239. (c) Berger, T.; Sterrer, M.; Diwald, O.; Knozinger, E.; Panayotov, D.; Thompson, T. L.; Yates, J. T, Jr. *J. Phys. Chem. B* **2005**, *109*, 6061.

(17) Wang, G. J.; Zhou, M. F. *Int. Rev. Phys. Chem.* **2008**, *27*, 1.

(18) Becke, A. D. *J. Chem. Phys.* **1993**, *98*, 5648.

(19) Lee, C.; Yang, W.; Parr, R. G. *Phys. Rev.* **1988**, *B37*, 785.

(20) Frisch, M. J.; Trucks, G. W.; Schlegel, H. B.; Scuseria, G. E.; Robb, M. A.; Cheeseman, J. R.; Montgomery. J. A., Jr.; Vreven, T.; Kudin, K. N.; Burant, J. C.; Millam, J. M.; Iyengar, S. S.; Tomasi, J.; Barone, V.; Mennucci, B.; Cossi, M.; Scalmani, G.; Rega, N.; Petersson, G. A.; Nakatsuji, H.; Hada, M.; Ehara, M.; Toyota, K.; Fukuda, R.; Hasegawa, J.; Ishida, M.; Nakajima, T.; Honda, Y.; Kitao, O.; Nakai, H.; Klene, M.; Li, X.; Knox, J. E.; Hratchian, H. P.; Cross, J. B.; Adamo, C.; Jaramillo, J.; Gomperts, R.; Stratmann, R. E.; Yazyev, O.; Austin, A. J.; Cammi, R.; Pomelli, C.; Ochterski, J. W.; Ayala, P. Y.; Morokuma, K.; Voth, G. A.; Salvador, P.; Dannenberg, J. J.; Zakrzewski, V. G. ; Dapprich, S.; Daniels, A. D.; Strain, M. C.; Farkas, O.; Malick, D. K.; Rabuck, A. D. ; Raghavachari, K.; Foresman, J. B.; Ortiz, J. V.; Cui, Q.; Baboul, A. G.; Clifford, S.; Cioslowski, J.; Stefanov, B. B.; Liu, G.; Liashenko, A.; Piskorz, P.; Komaromi, I.; Martin, R. L.; Fox, D. J.; Keith, T.; Al-Laham, M. A.;

Peng, C. Y.; Nanayakkara, A.; Challacombe, M.; Gill, P. M. W.; Johnson, B.; Chen, W.; Wong, M. W.; Gonzalez, C.; Pople, J. A. *Gaussian 03, Revision B.05*: Gaussian, Inc.: Pittsburgh, PA, 2003.

(21) Werner, H. J.; Knowles, P. J.; et al. Molpro quantum chemistry package; http://www.molpro.net).

(22) Chertihin, G. V.; Bare, W. D.; Andrews, L. *J. Chem. Phys.* **1997**, *107*, 2798.

(23) Zhou, M. F.; Zhao, Y. Y.; Gong, Y.; Li, J. *J. Am. Chem. Soc.* **2006**, *128*, 2504.

(24) Zhou, M. F.; Andrews, L. *J. Chem. Phys.* **1999**, *111*, 4230.

(25) Cramer, C. J.; Tolman, W. B.; Theopold, K. H.; Rheingold, A. L. *Proc. Natl. Acad. Sci. U.S.A.* **2003**, *100*, 3635.

(26) (a) Gong, Y.; Zhou, M. F. *J. Phys. Chem. A* **2007**, *111*, 8973. (b) Gong, Y.; Zhou, M. F.; Andrews, L. *J. Phys. Chem. A* **2007**, *111*, 12001. (c) Gong, Y.; Wang, G. J.; Zhou, M. F. *J. Phys. Chem. A* **2008**, *112*, 4936. (d) Gong, Y.; Ding, C. F.; Zhou, M. F. *J. Phys. Chem. A* **2007**, *111*, 11572.

(27) (a) Huber, K. P.; Herzberg, G. *Molecular Spectra and Molecular Structure. IV. Constants of Diatomic Molecules*; Van Nostrand Reinhold Co.: New York, 1979. (b) Andrews, L.; Spiker, R. C., Jr *J. Phys. Chem.* **1972**, *76*, 3208.

(28) Wells, J. R.; Weitz, E. *J. Am. Chem. Soc.* **1992**, *114*, 2783.

(29) Sun, X. Z.; George, M. W.; Kazarian, S. G.; Nikiforov, S. M.; Poliakoff, M. *J. Am. Chem. Soc.* **1996**, *118*, 10525.

(30) Ball, G. E.; Darwish, T. A.; Geftakis, S.; George, M. W.; Lawes, D. J.; Portius, P.; Rourke, J. P.; Bergman, R. G. *Proc. Natl. Acad. Sci. U.S.A.* **2005**, *102*, 1853.

(31) Andersson, M. P.; Uvdal, P. *J. Phys. Chem. A* **2005**, *109*, 2937.

JP804995D